Published by Avanti Publishers

International Journal of Petroleum Technology

ISSN (online): 2409-787X

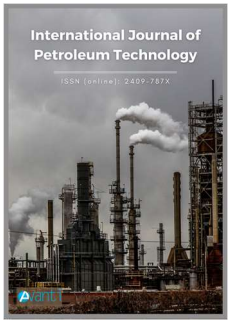

The Potential Use of Raw Iron Ore in Fischer-Tropsch Synthesis

Samuel Mubenesha[1,2], Chike George Okoye-Chine[2], Franscina Katuchero Ramutsindela[2], Joshua Gorimbo[2], Mahluli Moyo[2] and Xinying Liu[1,2,*]

[1]*Zhijiang College of Zhejiang University of Technology, Shaoxing, 312030, China*

[2]*Institute for Development of Energy for African Sustainability (IDEAS), University of South Africa, Florida, 1710, South Africa*

ARTICLE INFO

Article Type: Research Article

Keywords:
Catalyst costing,
Step-based method
Mechanical strength
Catalytic engineering
Fischer-Tropsch synthesis

Timeline:
Received: August 1, 2021
Accepted: September 15, 2021
Published: October 18, 2021

Citation: Mubenesha S, Okoye-Chine CG, Ramutsindela FK, Gorimbo J, Moyo M, Liu X. The Potential Use of Raw Iron Ore in Fischer-Tropsch Synthesis. Int J Petrol Technol. 2021; 8: 99-115.

DOI: https://doi.org/10.15377/2409-787X.2021.08.8

ABSTRACT

Fischer-Tropsch (FT) synthesis has been studied in the literature as a greener pathway to cleaner and sustainable hydrocarbons production. However, the cost to upscale laboratory FT formulations to pilot scale is significantly expensive. This work proposes a cheaper and scalable low-temperature FT modified iron ore catalyst that is mechanically suited for fixed bed reactors. The mechanical strength reported in this investigation was three times more than commercial alumina spherical pellets and, therefore, suitable for pilot scale scenarios. A manufacturing cost analysis of iron ore was estimated to be US$38.45/kg using the CatCost model, and the conventionally prepared iron catalyst was US$71.44/kg using the same model. The manufacturing cost estimations of modified iron ore were found to be 46% cheaper than a conventional commercial iron catalyst. The catalytic performance of the modified iron ore catalyst showed a CO conversion of 72.1% ±4.24, with WGS and C5+ selectivity 48.6% ±1.96 and 83.2% ± 5.24, respectively. These findings were comparable (both in CO conversion and product selectivity) to the ones reported by other researchers.

*Corresponding Author
Emails: liux@unisa.ac.za
Tel: +27722868656

1. Introduction

Catalyst cost is one of the crucial aspects to consider when upscaling new Fischer-Tropsch (FT) synthesis laboratory catalyst formulations to pilot scale [1-3]. The catalyst cost comprises the value of precursors, the catalyst preparation step, and the operational aspect [1, 4]. One way to reduce the cost of manufacturing new FT catalytic materials is to explore cheaper precursors without sacrificing their functionality. The use of slimes (a by-product of the beneficiation of iron from hematite ore) was examined as a more inexpensive alternative precursor for iron FT catalyst in this work. The re-utilization of this by-product is crucial for steel manufacturers to remain compliant with environmental regulations, increase their profitability and longevity [5].

Commercializing new catalysts is a tedious and complicated process that involves an interplay between the technical and economic factors before it is ready for industrial applications [1, 6]. The scaling up of novel catalysts comes with some risks, such as the difference in techniques used in the laboratory synthesis may not be applicable on an industrial scale [1-3, 6, 7]. Some of the other risks associated with upscaling existing laboratory catalyst formulations stem from the uncertainty in manufacturing the catalyst and predicting its performance on an industrial scale [1, 6]. The development and design of FT catalysts are not exempted from these risks, and consequently, a meticulous and systematic approach needs to be in place before upscaling FT catalytic materials [1, 6, 8-10].

The costs of upscaling should be factored into the conceptual and development phase [2, 3, 9, 10] to validate its implementation. Some publications in the literature show that the cost of manufacturing FT catalyst can contribute up to 9% of the total equipment cost [1] and thus should be lowered to make it more competitive, especially for small-medium FT practitioners. Moreover, some of the operational issues with scaling up catalysts are mechanical failure of solid catalysts, which leads to frequent plant shutdowns, putting much financial burden on FT specialists [6, 11-15].

The operational challenges that arise from the mechanical failure of solid catalysts in upscaled fixed bed operations lead to the formation of fines that change their shape and size [6, 11, 15, 16]. This, in turn, instigates significant pressure drop, uneven flow of fluid, heat, and mass transfer limitations resulting in insufficient catalyst activity [6, 11, 15, 17, 18]. Furthermore, the fragmentations of pellets subsequently plug units downstream [6, 11, 15, 16]; stopping operations altogether. Additionally, pellets that are not strong enough to withstand the mechanical stress before, during, and after reaction studies as they are challenging to handle [6, 11, 15].

Most recently, Bae *et al*. [19] proposed a promising and cost-effective iron ore FT catalyst approach alternative to conventional precipitated low-temperature Fischer-Tropsch (LTFT) iron-based with comparable FT activity to other traditional FT catalysts [19]. However, the study was more appropriate for laboratory operations and did not consider the mechanical strength of the catalyst, which is crucial for upscaled fixed operations, as mentioned earlier. Therefore, this study uses the successful catalyst formulation proposed by Bae *et al*. [19]. However, it improves it by considering the mechanical strength of the catalyst and using slimes instead of high-grade iron ores, which are relatively more expensive.

The debottlenecking of the capital costs involved in upscaling new and existing FT catalysts is crucial to keep up with projected energy demands by the World Economic Forum [20]. Furthermore, the need for sustainable and clean energy is expected to grow proportionally to the population as more stringent restrictions are put on the use of fossil fuels [20-24]. Therefore, necessitating the need for accelerated implementation of small-medium FT operations to keep up with this trend, especially in African setups. This is bolstered by the World Economic Forum findings that show Africa has the fastest population growth rate globally, and its population would have tripled by 2050 [20, 24]. Therefore, it is imperative to fast-track the development of cheap and scalable FT catalysts to keep up with the African projected energy demands.

As a result, the crux of this investigation was aimed at developing a cheap and scalable FT iron ore catalyst, using the step-based method recommended by Baddour *et al*. [1] as an accurate way to cost its manufacturing. The step method in CatCost uses a simplified approach to process production estimations for novel catalysts in

which all capital and operating costs are associated with a process step at a specified production scale. CatCost estimations have been reported to be within ± 20% with market prices and thus deemed appropriate for techno-economic analysis of new pre-commercial catalysts [1]. CatCost ability to be customized to suit new catalysts was one of the main factors that made it attractive for this work. This manuscript proposes iron ore slimes as a cheaper alternative to a conventional precipitated iron catalyst modified to suit typical FT reaction conditions. The competency of this iron ore catalyst was validated by evaluating its catalyst performance and estimating the upscaling cost of manufacturing. These findings were then compared to conventional FT iron catalysts from an economic and technical standpoint to build a strong case as a viable option for small-medium FT practitioners.

2. Methodology

2.1. Materials

Anglo American supplied iron ore (Fe_2O_3) powder from their Sishen tailing Dams based in Northern Cape, South Africa. The iron ore used in this work is a by-product of the direct reduction process of iron ore into metallic ore. Copper (II) nitrate trihydrate [$Cu(NO_3)_2.3H_2O$] and potassium carbonate (K_2CO_3) were purchased from Sigma-Aldrich, South Africa, while bentonite binder was purchased from Gw mineral Resources, Johannesburg, South Africa.

2.2. Catalyst Preparation

The catalyst was synthesized according to the slurry phase impregnation method reported in the literature [19]. This involved weighing 1 kg of Fe_2O_3 powder with a particle size range of 60–80 microns and then making a slurry in a 5 L beaker by adding an appropriate amount of de-ionized water. After that, 42.64 g of $Cu(NO_3)_2.3H_2O$ was added, followed by 84.36 g of K_2CO_3. The catalyst promotion additions were added to give an atomic ratio percentage relative to elemental iron of 100Fe/3.8Cu/9.6K. The role of the Cu promotion was to reduce the induction period of the promoted iron ore, while that of the K promotion was mainly to facilitate the carburization of the iron ore phase to enhance the overall catalytic performance [25]. Subsequently, the slurry was stirred for 2 hours and then dried in an oven at 120 ^oC for 24 hours and then calcined for 4 hours in atmospheric air at 400 ^oC in a muffle furnace.

2.3. Pelletizing of Promoted Iron ore

The powder 100Fe/4.5Cu/5.5K was pelletized in a rotating disk using bentonite as the binder. The binding additions were varied by 10, 15, and 20 wt.% to determine the optimum catalyst-binder combination for the highest mechanical strength. The first batch for pelletization was prepared first by weighing 300 g of bentonite (10% binder addition) and adding to 3 kg of catalyst powder labeled 100Fe/4.5Cu/5.5K. The mixture was thoroughly mixed and then fed to the pelletizer (rotating drum). Water was sprinkled to initiate the sticking of fine particles and subsequent coalesce of seeds. The formed pellets were then sieved, and the undesired particle size range was re-loaded to the pelletizer to achieve the designed particle size range (2–3 mm). The same procedure was followed to prepare the catalysts containing 15% binder (450 g of bentonite addition) and 20% binder (600 g of bentonite addition). For convenience, the samples have been denoted as 10B for the catalyst containing 10% bentonite binder,15B for the catalyst containing 15% bentonite binder, and 20B for that containing 20% bentonite binder. Figure **S1** depicts the overall schematic representation of the catalyst development for this work.

2.4. Characterization of Catalyst

The physical properties such as surface area, pore-volume, and pore diameter were analyzed using a Micromeritics **ASAP Tristar II** Analyzer. The reducibility of the catalyst was studied using temperature-programmed reduction (TPR) performed with the Micromeritics AutoChem 2950 HP. The crystallinity and chemical composition of the as-synthesized catalyst was studied using a Rigaku X-ray Powder Diffractor with scans performed at 2θ = 0–90^o using Cu Kα radiations. The elemental analysis of all catalyst systems was done using X-ray Fluorescence with the PANalyticall **Axios Fast 1 MagiX PRO X-Ray** Fluorescence Spectrometer.

2.5. Mechanical Testing of Pellets

A single pellet test is a useful technique for studying the mechanical strength of a catalyst pellet; it refers to the external load (in Newtons) a single pellet can withstand before it fractures [13, 15, 17, 18, 26]. Parameters such as the pellet size, loading mode, loading speed, temperature, and humidity are kept as fixed variables to allow for comparison between samples [15, 17, 18] . The single pellet test was carried out by using a force gauge (FG-5052 model) with a maximum load measurement of 300N/pellet. The pellet crushing strength can be expressed in Pascals (Pa) by the following equation (1);

$$\tau_S = \frac{2.8 \times Force(N)}{\pi d^2} \quad (1)$$

Where:

τ_S is the crushing strength in pascals,

d is the diameter of the spherical particles (meters).

Force (Newtons) is obtained from the force gauge.

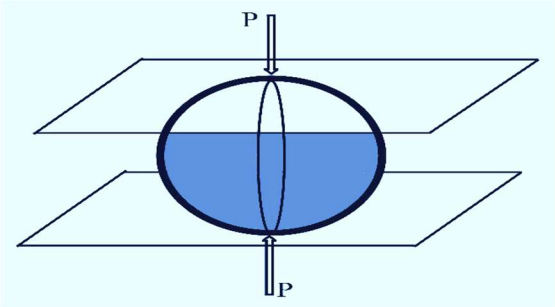

Figure 1: Single Pellet Crushing test. Reproduced with permission from Badgoga *et al*. [13].

Badgoga *et al*. [13] recommended that spherical catalyst pellet should typically exhibit 620 kPa single pellet crushing strength or more for use in fixed bed reactors at 20 bar and 270 ^{o}C. Twenty pellets were randomly sampled from each catalyst batch and tested with a force gauge.

Single pellet crushing strength tests on spherical pellets yield scattered strength data, which usually does not follow a normal distribution [15, 17, 18]. This effect leads to difficulties when predicting the mechanical failure of solid catalysts [15, 17, 18]. In this case, the Weibull distributions provide a facile way of predicting the probability of failures and reliabilities of skewed strength data. Comparative analysis between different solid catalysts to determine the optimum mechanical strength for a specific application using the standard deviations and mean are inaccurate to use as a benchmark, and thus the median rank was proposed [15, 18, 27]. The batch with the highest mechanical strength mean is a more reliable solid catalyst under specified reactor conditions. Therefore, this batch will be an excellent batch to consider for further designing and manufacturing. However, it does not necessarily mean that it is the most suitable catalyst commercially. Consequently, the mechanical reliability of solid catalysts is much more useful to consider and ensure their suitability for commercial applications.

In this context, mechanical reliability is the probability that a catalyst system will continue to perform under specific process conditions. Mechanical reliability is obtained from probability distributions under specific loads by Weibull distribution statistics, and it is a better way to predict catalyst failures at various stresses [15, 18, 27]. The most common form of Weibull statistics used for this measurement is the two-parameter Weibull distribution given by;

$$P_f(F) = 1\text{-}\exp[-(F/F_o)^m] \quad (2)$$

Where:

P_f is the probability of failure,

F is the load at failure (Kgf),

m is the Weibull modulus.

F_o refers to the Weibull size parameter, a volume-dependent scale parameter relating to the fracture stress with a failure probability of 63.2% [15, 18, 27]. The Weibull two-parameter distribution is valid when constant volumes are used for all tested pellets [15, 18, 27].

Linear regression is used to estimate the Weibull parameters in equation (2) and is linearized by taking logarithm twice[15, 18, 27] . Equation (2) in its linearized form becomes;

$$Y=\ln\ln\left[\frac{1}{1-P_{f(F)}}\right] = mlnF - lnF_O \tag{3}$$

A plot of Y versus *lnF* yields a straight line with a slope m and a y-intercept -*lnF*$_o$. *lnF* and Y in the equation are independent and depend on variables, respectively. *F* is the single pellet crushing strength measured experimentally. The Weibull modulus, m, is the shape parameter that determines the scattering extent of the failure strength, and F_o is the scaling parameter obtained from either the probability of the failure curve or equation (4) [15, 18, 27];

$$P_f(F) = \frac{i-0.5}{n} \tag{4}$$

Where P_f is the probability of failure and the i^{th} is the ranked single pellet strength measured by force gauge, and n is the sample size being tested [15, 18].

2.6. FT Synthesis

Catalyst evaluation was carried out in a fixed bed reactor (FBR) of 204 mm length and 8 mm internal diameter. All experiments were carried out at a gas hourly space velocity (GHSV) of 3.6 NL/g_{cat}-h, the pressure of 20 bar, reaction temperature of 270 ^oC, and feed H_2/CO ratio of 2.0. Before the FT reaction, the catalyst was activated for 12 hours at 350 ^oC with syngas (H_2/CO = 2.0, 1.8 NL/g_{cat}-h) at 1 bar (abs). All products were analyzed by an online gas chromatograph (GC) equipped with a flame ionization detector (FID) and two thermal detectors (TCDs).

The data collected from the online GC were quantitatively processed. 10 vol % of N_2 contained in syngas feed of FT experiments was used as the internal standard for the mass balance calculation. Once the molar flow rates of the various reactants and products were determined, then conversions and mass balance calculations were calculated. Mass balance calculations, including the conversion of reactants CO and H_2, were determined using the equations below;

$$\%\ CO = \frac{F_{in}X_{co,in} - F_{out}X_{co,out}}{F_{in}X_{co,in}} \tag{5}$$

Where:

$X_{co,in}$ and $X_{co,out}$ are the molar fractions of CO in the reactor inlet and outlet, respectively,

F_{in} and F_{out} are the molar flow rates of gas in and out of the reactor, respectively.

The CO consumption rate, (mol/(min g-cat), was calculated using the following equation;

$$r_{CO} = \frac{F_{in}X_{co,in} - F_{out}X_{co,out}}{m_{cat}} \tag{6}$$

Where m_{cat} is the mass of the catalyst used in the reaction, in grams.

The rate of formation of product θ_i, mol/(min.g.cat) mathematical represented as;

$$r_{\theta_i} = \frac{F_{out}X_{\theta_i,out}}{m_{cat}} \tag{7}$$

Where $X_{\theta i,out}$ is the molar fraction of θ_i in the reactor outlet gas stream. The product selectivity for species θ_i, $Sel(\theta_i)$ is calculated on a mole of carbon basis, as follows:

$$\boldsymbol{Sel}(\theta_i) = \frac{[nC]_{\theta_i}}{-r_{CO}\, X\, t\, X\, m_{cat}} \tag{8}$$

Where $[nC]_{\theta_i}$are the moles of carbon in species θ_i contained in a sample of the exit of the reactor collected over time.

2.7. Step-Based Catalyst Price Estimation

In this section, the step method proposed by Baddour *et al*. [1] was used to estimate the costing of catalyst synthesis for both modified iron ore and a conventional precipitated iron catalyst. After that, a comparative analysis was done to validate the upscaling of the modified iron ore as a viable and cost-competitive alternative to the conventional one. This was achieved by directly entering relevant inputs such as catalyst precursors, required amounts, and appropriate equipment list for processing steps to generate the unit cost of production for each catalyst synthesis case using CatCost. It is important to note that the additions of precursors were added according to their stoichiometric ratios to ascertain the mass required to achieve the specified catalyst formulations.

This estimation approach is based on prices used by contract catalyst manufacturers when they quote for their paid services and is useful for catalyst developers of new materials and limited information to forecast the catalyst synthesis cost accurately [1]. A price estimation using the step method requires information on both the catalyst synthesis (synthesis inputs) and the application of the catalysts (Business inputs). These inputs are based on the laboratory scale synthetic procedure developed by the researcher or from the literature. Moreover, various precursors were added to the material library of CatCost using prices from Sigma, and other credible suppliers as the original material library did not have some of these entries. The production scale of the catalyst synthesis for this investigation was 1 ton/day (Small scale), and all the costs were expressed in US dollars for convenience.

The inputs can be divided into synthetic inputs and business as shown below in Figure **2**.

3. Results and Discussions

The iron ore catalyst pellets' physio-chemical properties are discussed in this section and correlated to their catalytic performance under FT conditions in a laboratory fixed bed reactor to ascertain their functionality in pilot-scale scenarios. After that, the cost to manufacture the proposed catalyst was estimated using a facile step-based method compared to a conventional catalyst synthesis route. The comparison will help validate the proposed iron ore catalyst's applicability for small-medium FT practitioners with a limited budget at the pre-commercial stage of catalyst development. For convenience, the promoted catalyst before binder addition is denoted as 0B, while the pelletized promoted catalysts after binder additions are 10B, 15B, and 20B.

3.1. Statistical Analysis of Mechanical Strength Results

The pelletized catalysts' mechanical strength is determined in this section and then analyzed statistically.

3.1.1. Single Pellet Crushing Tests Results

The skew single scattered pellet crushing strengths data presented in Tables **S1** and **S2** were statistically analyzed (Table **S3**) using the Kruskal Wallis test to determine if the batches are significantly different [30]. Moreover, the Kruskal Wallis test is an alternative to the one-way ANOVA statistical tool. It is suitable for data with independent variables that are ordinal (ranked) and cannot be analyzed using the one-way ANOVA test [30]. The Chi-squared of 29.0844, df = 2, and P-value < 0.05 from Table **S3** means we can reject the null hypothesis and conclude that a single pellet crushing test from each batch has a significant difference.

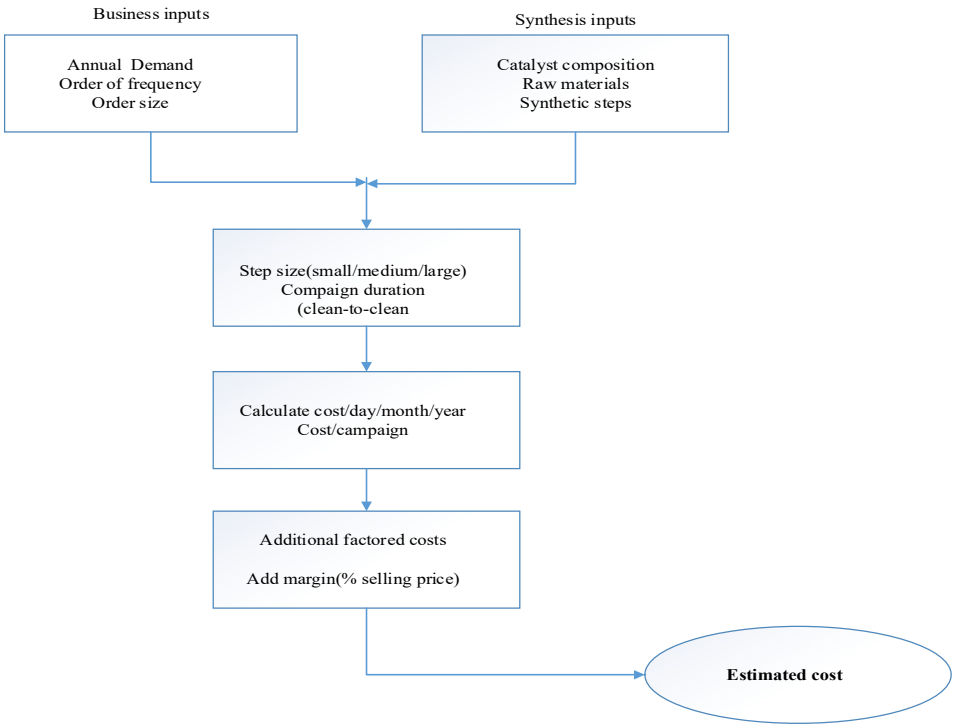

Figure 2: Schematic representation of the step method process used to estimate costs at a contract catalyst manufacturer. Reproduced with permission from Baddour *et al*. [1].

After the Kruskal test reveals that the groups are significantly different, there is a need to perform a Post hoc Dunn test to determine which amongst the sampling groups is different [30]. Based on the results presented in Table **S3** after completing the test above, the null hypothesis for comparing 10% binder loading with 15% and 20% loadings was invalid because the p-value is less than the estimation of 0.05. Therefore, the 10% binder addition is significantly different from the rest based on the p-values, and we can conclude it gave the best mechanical strength. Consequently, we have not only considered the means but also medians by performing these two hypothesis tests [15, 27].

3.1.2. Weibull Statistics

Figure **3** represents all the shaped catalysts' probability failures curve for this work and depicts that 10% binder pellets (10B) can withstand a higher mean compressive strength of 1832.67 kPa than 15B and 20B pellets which agrees with the Post hoc Dunn test. The 1832.67 kPa is also superior to the 620 kPa recommended for fixed bed operations [13], as cited earlier. The Weibull statistics provided relevant information to compare all three catalyst systems and facilitate selecting the catalyst that will be the most suited for our scenario [15, 18].

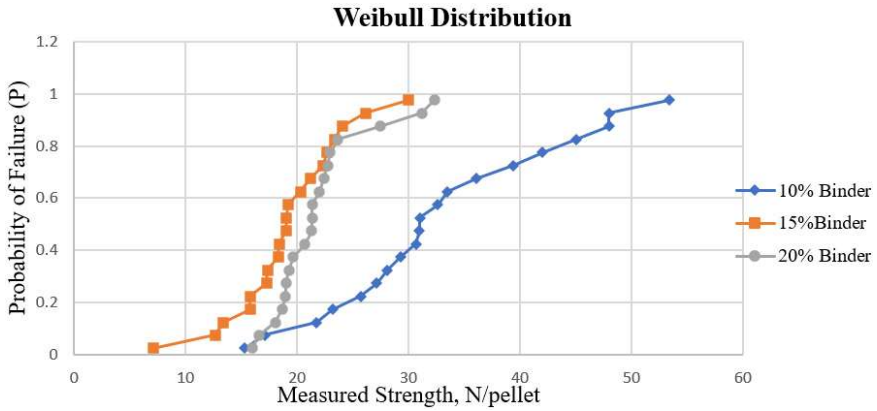

Figure 3: Weibull Distribution curve for pelletized catalysts.

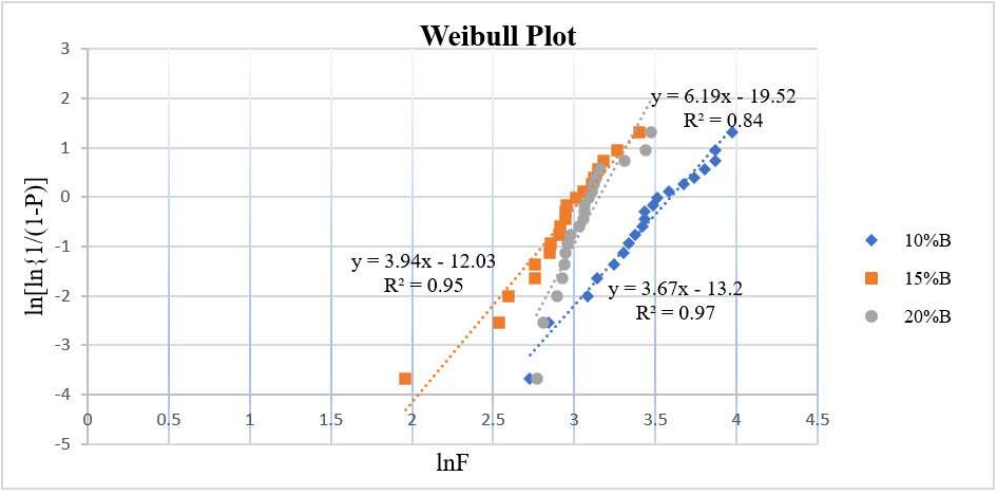

Figure 4: Weibull Plots of all pelletized catalyst systems.

Table 1: Summary of Mechanical strength testing Parameters.

Binder Additions by Weight Percentage (%)	Crushing Strength		Weibull Modulus	R^2	Weibull Size Parameter, F_O(kPa)
	Mean (kPa)	Standard Deviation (kPa)			
10B Fe/K/Cu	1832.67	581.00	3.67	0.97	2266.04
15B Fe/K/Cu	1068.96	279.08	3.94	0.95	1180.37
20 B Fe/K/Cu	1213.24	239.53	6.19	0.84	1304.59

Based on findings from Figures **3** and **4**, we chose 10B as the best catalyst for laboratory FT reaction studies. This data was substantiated by the post hoc analysis reported earlier without considering the mechanical reliability aspect (Figure **4** and Table **1**). The decision was made because, in scenarios where FT runs were for short periods, the catalysts' reliability was not crucial. However, for future pilot-scale studies, the modulus' mechanical reliability parameter will be considered when applying the various catalysts with binder variations on upscaled fixed bed reactors linked to functionality for FTS. Weibull statistics was a good fit for scattered single pellet crushing strengths and substantiated by the Pearson's coefficients being all very close to 1 [15, 18]. The 10% binder catalyst was the most robust amongst all pelletized catalysts and therefore selected for characterization and FT reaction studies.

3.2. Characterization Results Related to FT Catalysts Performance

The physical and textural properties of the modified iron ore catalyst probed the changes it undergoes throughout the catalyst development.

Table **S6** represents XRF results used to study how the addition of the binder affected its chemical compositions during the catalyst synthesis. The promotion of iron ore with Cu and K has been shown in previous studies[11, 19, 25] to improve the overall catalytic activity of fresh iron ore. Therefore, this study also added these dopants to ensure a reasonable outcome.

Table **S6** shows that the binder addition decreased the iron content in the precursor by only 11%. In contrast, the potassium content (K_2O) increased significantly after promotion from 0.04 wt% to 6.41 wt%, which was expected but only dropped by 18% after the binder addition. The CuO remained unchanged after binder addition, as shown in Table **S4**.

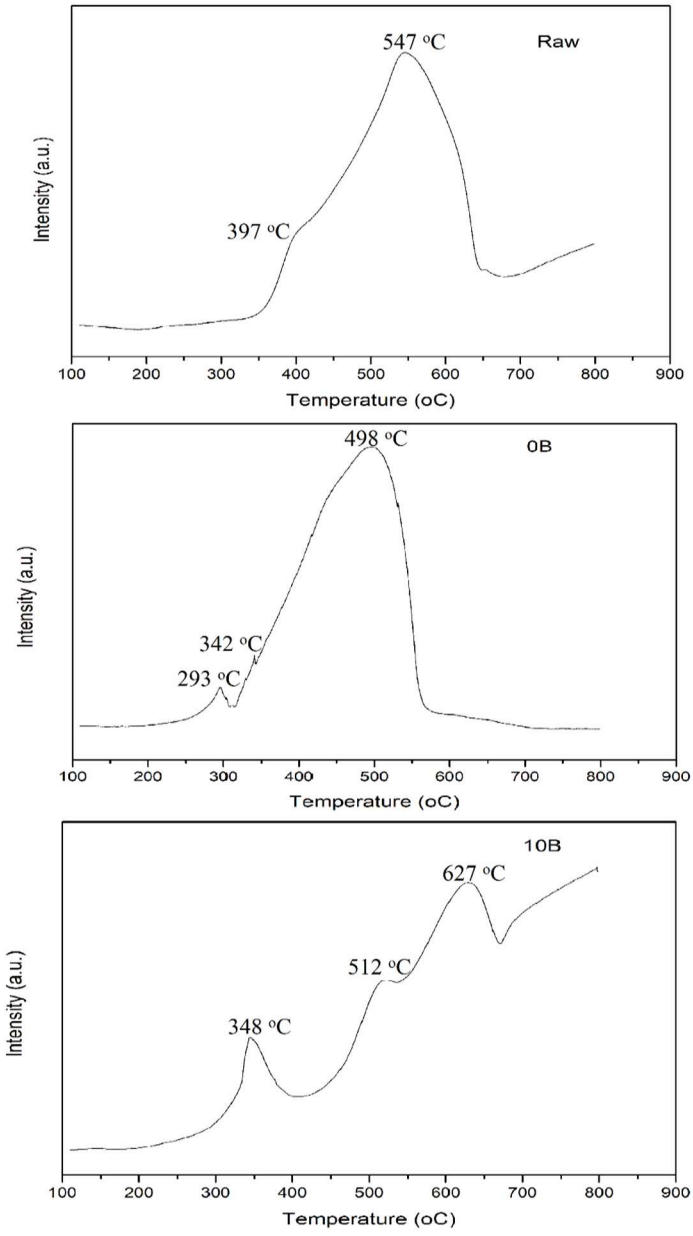

Figure 5: H_2-TPR profiles of the catalysts.

A two-step reduction profile of the hematite raw iron ore (Fe_2O_3) was observed, as shown in Figure **5**. The first reduction step occurs at a temperature of ~397 °C; this peak relates to the reduction of hematite (Fe_2O_3) phases to Magnetite (Fe_3O_4) phases. The second peak that appears at ~547 °C is ascribed to the reduction of Magnetite (Fe_3O_4) phases to metallic iron (Fe) phases. These reduction temperatures are slightly higher than the ~325 °C [19] previously reported in the literature for fresh iron ore and could be attributed to the ores from different sources. Therefore, varied elemental compositions and reducibility.

The promoted iron ore showed a similar two-peak profile of the fresh iron ore. However, its peaks were observed to occur at lower temperatures than the fresh iron ore catalyst. The first reduction peak at ~293° C was ascribed to the reduction of CuO to Cu [13], which confirms that the addition of Cu promotes the reduction of iron ore phases. This was bolstered by the peak shift of the hematite phase change in the raw iron ore from ~397 °C to ~348 °C in the promoted iron ore (0B). This small shoulder peak at ~350 °C was 47 °C lower than the raw iron ore. Also, the promotion of the raw iron ore shifted the reduction temperature of the magnetite phase to the metallic iron phase from 547 °C to 498 °C in the promoted iron ore (0B). Thus, confirming the positive effect of copper on fresh iron ore [25].

The presence of a 10% wt/wt bentonite binder on the promoted iron ore (10B) resulted in an additional peak on the TPR profile compared to raw iron ore and the promoted catalyst (OB). Similar reduction behavior has also been reported in the literature after an identical binder addition [13]. The first peak corresponds to the phase change of hematite (Fe_2O_3) to magnetite (Fe_3O_4), whilst the second peak is the magnetite (Fe_3O_4) phase change to metallic iron (Fe). The third peak is ascribed to the Fe-SiO_2 and Fe-Al_2O_3 interactions; refer to Table **S7** for the elemental composition of the binder. The hematite reduction peak into magnetite was like the promoted ore (0B) and occurred at ~348 ^oC. A slight shift of reduction to the right to ~512 ^oC was observed for the magnetite phase change into metallic iron after the binder addition. The last peak occurring at ~627 ^oC was attributed to the Fe-SiO_2 and Fe-Al_2O_3 interactions[14, 19]. The binder addition did not significantly change the reducibility of the promoted iron ore and was necessary for this investigation.

A thorough analysis of catalyst systems' crystallinity before and after binder addition was performed with X-ray diffraction (XRD). The XRD patterns generated by powder diffractor using Cu Kα radiations are delineated in Figure **S2**, together with phase determination. The crystallite size of oxides present in the selected catalyst system was also determined by Scherrer's equation and presented in this section. The XRD patterns displayed show various intensities and occurrences at different peak angles, suggesting a myriad of phases present in the samples. The prominent peaks occurring at 2θ = 34.4^o and 40.0^o confirm the presence of hematite (Fe_2O_3) in all samples and correspond well with the ones in the literature reported to occur at 33.0^o and 40.8^o [13]. The tenorite (CuO) occurring at 2θ of about 39.0^o and for potassium aluminum silicate at 2θ of about 32.5^o were identified via XRD analysis and confirmed the successful deposition dopants unto the catalyst's surface for shaped materials [13].

The crystallite size of the active phase (hematite) in each sample was calculated and displayed in Table **2**. The crystallite of the hematite phase in the raw iron ore sample was 41.2 nm and was like the 47 nm in the literature [14]. It is clear that the crystallite size of the hematite phase in the 0B remained the same after calcination and was expected. Similarly, the binder addition did not change the crystallite size (46.23 nm) of the iron ore catalyst (10B), as shown in Table **2**. The XRD spectra also reveal that the binder addition did not change the proposed catalyst's crystallinity, as shown in Figure **S2**.

The fresh powder iron ore sample shows a smaller pore size distribution than the 10B catalyst, as shown in Figure **S3**. However, the catalyst without the binder (OB) incremental pore areas and pore diameters data points were not enough to plot a line graph. Therefore, the blocking pores of the powder catalyst were believed to have caused this trend. Conversely, Figure **S3** reveals particle agglomeration and unblocking their pores by the binder addition, which is similar to the trend reported by Seo *et al*. [14]. Additionally, the pelletized catalyst's pore size distribution was mostly around 40–50 nm (mesoporous), confirmed by the peaks at those areas in Figure **S3** and Table **2**.

Table 2: Summarized textural and physical properties of the iron ore catalyst from its precursor to the pelletized form.

Catalyst	BET Surface Area (m^2/g)	Pore Volume (cm^3/g)	Average Pore Diameter (nm)	Average Crystalline Size (nm)
Raw iron ore	2.07	0.0023	9.72	41.19
0B	0.44	0.00018	7.15	41.63
10B	1.22	0.0033	43.85	46.23
Binder	73.79	0.073	8.30	-

Table **2** summarizes the catalyst's textural properties changes during its synthesis. It is evident from the summarized results that there was a drastic drop in BET surface area and pore volume of the precursor after promotion by 79% and 92%, respectively. This was attributed to the blocking of pores during the promotion of the raw ore and thus needed enhancement before it is applied for FT. On the other hand, a comparison between the 0B and the 10B catalysts, seen in Table **2**, indicates an improvement in the BET surface area and pore volume of 1.22 m^2/g and 0.0033 cm^3/g, respectively, credited to the binder addition [13], which unblocked the pores of its

precursor and is supported by the pore size distribution curve in Figure **S3**. Furthermore, the improvement in surface area and pore volume was ascribed to the binder's superior textural properties of 73.79 m^2/g and 0.073 cm^3/g, respectively, as shown in Table **2**.

On the contrary, the pelletized catalyst (10B)'s textural properties in Table **3** showed inferior properties compared to similar work reported in the literature, owing to the difference in raw iron ore sources. Natural iron ore was sourced locally from Sischen Mines, South Africa, while the one reported in the literature was from South America [19, 28]. The surface area and pore volume of the promoted pelletized catalysts ore were measured to be 1.22 m^2/g and 0.0033 cm^3/g, respectively, which was much lower than 84.7 m^2/g and 0.312 cm^3/g to the promoted iron ore in the literature delineated in Table **3**. These textural properties were also not comparable to precipitated iron catalysts reported in the literature [19] but exhibited similar FT activity to both catalyst systems and justified its application for this type of work.

Table 3: A comparison of chemical composition, textural properties, and average crystallite size of 10% binder promoted iron ore versus similar catalyst systems in the literature.

Catalyst	Chemical Composition (g/100 Fe)[a]			Textural Properties[b]			Average crystallite Size (nm)[c]	Category (Literature or Present work)[d]
	Fe	K	Cu	BET Surface Area (m^2/g)	Pore volume (cm^3/g)	Average Pore Size (nm)		
PIO-CAT	100	9.62	3.83	1.4	0.004	40.7	45.5	Present Work
IO-CAT	100	5.28	5.43	84.7	0.312	14.7	21.5	Literature[19]
PFe-CAT	100	5.25	5.09	135.0	0.326	10.8	12.5	Literature[19]

[a]Analyzed by XRF; [b]Analyzed by N_2 Adsorption; [c]XRD Average crystallite size; [d]Category; **PIO-CAT** denotes the promoted iron ore pellets while **IO-CAT** promoted ore without any binder and **PFe-CAT** iron catalysts prepared by precipitation by the same researchers.

3.3. Catalyst Performance

The catalyst evaluation of the 10% binder pellets was performed by looking at the CO conversions, product selectivity, and CO rates.

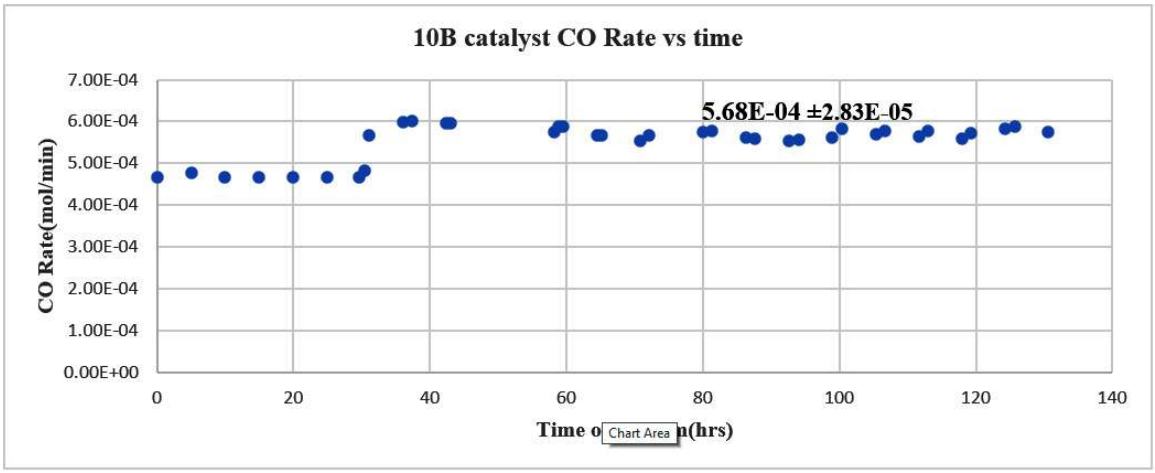

Figure 6: CO rate of 10% binder catalyst after 131 hours time on stream. Reaction conditions: 270 °C, 20 bar, GHSV of 3.6 NL/gcat-h (H_2/CO=2.0).

The CO consumption rate of the 10% binder catalyst gradually increases and then starts to stabilize at a TOS of about 65 hours and maintains a steady state for the rest of the experiment. This is attractive because it shows that the proposed catalyst is stable for most of the time on stream and beneficial for this study where upscaling existing laboratory catalyst formulations is the main objective. The average CO rate yielded by this catalyst was 5.68E-04 mol/min.

Table 4: The FT catalysts performance and reaction conditions summary of 10B catalyst versus other iron-based catalyst reported in the literature between 66–114 hours TOS.

Catalysts	Temp (°C)	Reaction conditions			Conversion CO (mol%)	Selectivity (%)				Class
		GHSV (NL/g-cat.h)	Pres (bar)	H_2/CO		CO_2	CH_4	$C_2–C_4$	C_{5+} (%)	
10BCAT	270	3.6	20	2.0	72.1	48.6	5.00	17.4	83.2	Present work
IO-CAT	275	2.8	15	1.0	75.4	42.6	9.05	20.0	71	Literature [19]
PFe-CAT	275	2.8	15	1.0	85.0	44.2	9.25	22.9	68	Literature [19]
PFe-CAT1	270	2.8	13	0.7	78.7	47.5	36.0	-	64	Literature [19]
PFe-CAT 2	270	2.0	13	0.7	74.7	47.7	5.8	21.7	72	Literature [19]

IO-CAT denotes promoted ore prepared by slurry phase impregnation with no binder, and **PFe** denotes conventional LTFT catalysts prepared by precipitation.

The 10B catalyst's CO conversion of 72.1% tabulated was comparable to the ones reported by Bae *et al*. [19] for both modified iron ore and precipitated iron catalysts, which ranged between 70–85%. This outcome demonstrates its promising potential as an effective FT catalyst for pilot-scale operations. Moreover, the 10B catalyst had a lower selectivity towards undesirable methane, which was found to be 5% which is very similar to the 5.8% of a conventional precipitated iron catalyst that operated at similar process conditions (see Table **4**) reported in the literature [19]. Moreover, low methane selectivity favoured the total selectivity towards C_{5+} hydrocarbons. It was evident in this study, 10% Binder catalyst (present study) recorded a high of 83.2% in comparison to the iron ore catalyst [IO-CAT], which was reported to be 71% between 66–114 hours [19]. The same work reported their conventional iron-based catalyst to have a C_{5+} hydrocarbons selectivity of 68% [19], which falls in a similar range as our present study catalyst yielded. Moreover, the C_{5+} hydrocarbon selectivity of 83.2% is identical to the ones reported by Badgoga *et al*. [13]. They also used bentonite as a binder for shaping an iron-based catalyst into spherical pellets with similar binder ratios. The C_{5+} hydrocarbon selectivity was in the range of 80–85% after 70 hours, suggesting that bentonite (binder) positively affects the C_{5+} hydrocarbon selectivity of iron-based FT catalysts. The $C_2–C_4$ selectivity of the proposed catalyst was similar to other iron ore and precipitated iron catalysts, as shown in Table **4**. The present study reported an average of 17.4% selectivity towards $C_2–C_4$ hydrocarbons between 66–114 hours on stream. Conversely, the high selectivity towards CO_2 is usually associated with a high water-gas shift reaction, which is a characteristic of iron-based catalysts in general, and this study was not an exception. The current pelletized promoted iron ore catalysts exhibited a CO_2 selectivity within the range of 42–48%, which agreed with other iron-based LT-FTS catalysts reported in the literature[13, 14, 19, 25, 28], recording CO_2 selectivity of 48.6%.

3.3. Catalyst Manufacturing Cost Analysis

The cost analysis of the proposed iron ore catalyst manufacturing is presented by considering all the reagents and process steps involved in the catalyst synthesis. A comparative analysis is then done with a conventional precipitated catalyst synthesis to validate its applicability.

Table **5** shows the precursors and their unit costs computed according to the stoichiometric ratios of each catalysis synthesis scenario for 1 ton/day. The material consumption for the conventional precipitated iron catalyst was calculated based on stoichiometric ratios of 100Fe/5.25Cu/5.09 K/ 8.77Si, as reported by Bae *et al*. [19]. Then the material consumption was tabulated to demonstrate how they contributed to the overall estimation [1-3, 29]. The precursors for the proposed modified iron ore were fresh iron ore(hematite), copper (II) nitrate trihydrate, potassium carbonate, and bentonite binder. The conventional precipitated iron catalyst's precursors were iron (III) nona nitrate, copper (II) nitrate trihydrate, potassium carbonate, and silica gel. The processing step was populated in CatCost according to the procedure described by Baddour *et al*. [1]. Other expenses such as admin, research, spent catalyst recovery, and selling margin was incorporated in the final costing of the conventional iron catalyst preparation and added to the other cost to get an aggregate catalyst manufacturing cost [1-3, 29].

The final step in the costing of catalyst synthesis includes other expenses such as administrative fees, research-related costs, spent catalyst recovery, and selling margins. The margins are included to make the pricing more realistic and reflect what happens in the industry [1-3, 29]. For example, the catalyst manufacturing unit internally would be a customer of the chemical plant's reaction section and would want to recover some of the capital invested in building the plant. In our case, 50% of the suggested selling margin for the proposed catalyst was considered and added to this section's overall expenses. A summative cost comparing the modified iron ore and conventional iron catalyst synthesis is presented in Figures **7**, **8**, and **9**, respectively.

Figure **7** and **8** shows the segmentation of costs for each catalyst synthesis case, and it clear that there is no significant difference between the two. The proposed modified iron ore's process synthesis step contributed about 48% of the overall manufacturing cost, while the convention precipitated iron catalyst contribution was 51% which was expected. The precursor input cost for both cases was 19% and 18%, while the other expenses were 32% and 31%, respectively.

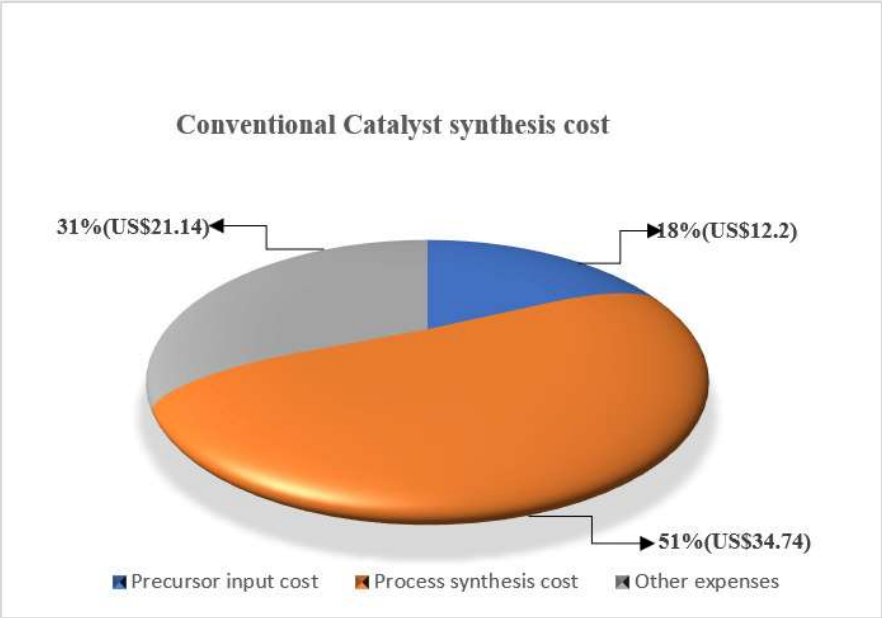

Figure 7: A graphical segmentation of conventional precipitated iron catalyst synthesis costing.

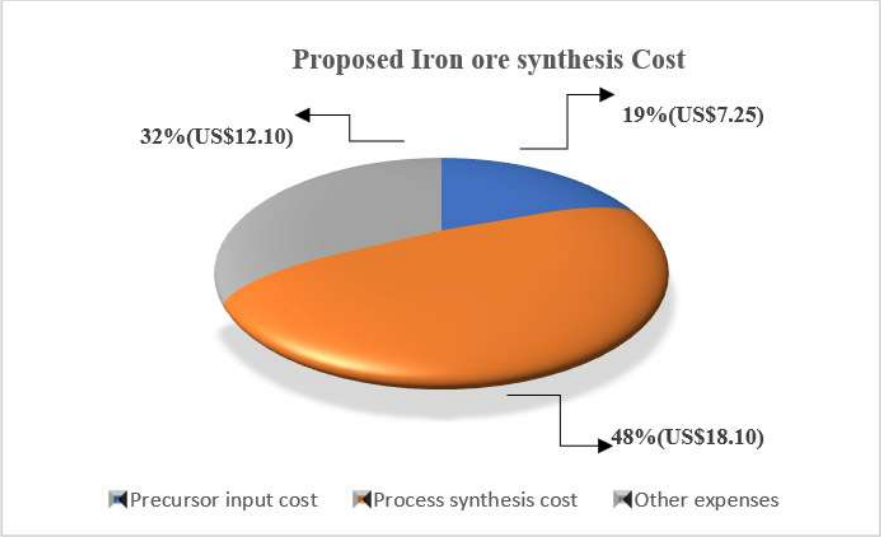

Figure 8: A graphical segmentation of the proposed iron ore synthesis costing

The summation of all these costs yielded an estimation for conventional precipitated iron catalyst manufacturing of **US$71.44/kg,** as shown in Figure **9**. It is clear to see that the total catalyst cost of manufacturing for the iron ore is 46% (**US$38.45/kg)** cheaper than the conventional one and thus justified its application as a viable alternative for the FT industry. This significant difference in cost between the two was attributed to the cheaper iron ore precursor than the traditional iron catalyst. The latter also had a much more expensive binder, 200 times than the proposed iron ore, as delineated in Table **5**. The precursor input costs, process synthesis costs, and other expenses for iron ore were **US$7.25/kg, US$18.1/kg**, and **US$13.1/kg,** respectively, which was significantly lower than the **US$12.2/kg, US$34.74/kg** and **US$24.5/kg** reported for the traditional iron catalyst. In both instances, the process synthesis step is the largest contributor to the overall cost, as expected, because of all the extra equipment needed to successfully synthesis each catalyst.

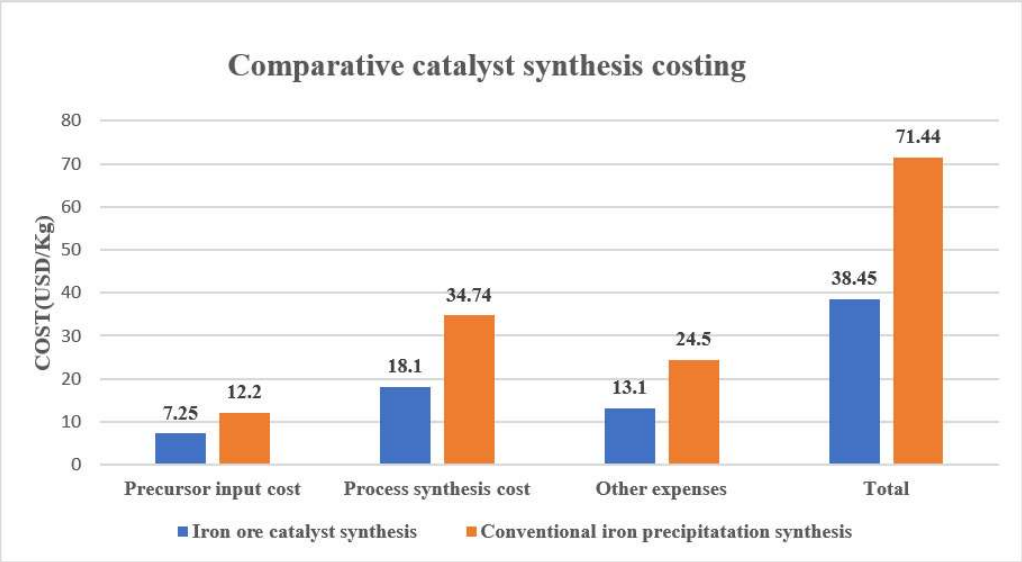

Figure 9: A comparative analysis of Catalyst manufacturing cost

The spent catalyst costs in these valuations can either have a negative or positive sign depending on whether it is a return or an expense to the catalyst manufacturer [1]. In our case, both scenarios were positive, which suggests that it is an added cost. Still, the proposed iron ore synthesis route's spent catalyst cost was almost twofold cheaper than the typically precipitated iron catalyst synthesis route. The decision to landfill the spent catalysts in both cases was the apparent decision based on the recovery fees involved. Neither catalyst was expected to have a substantial sale or metals recovery value, as shown in Table **5**. The proposed iron ore's recovery fee of **US$1.04/kg** was nearly four times higher than the **US$3.83/kg** of its counterpart, as shown in Table **5**. The estimations displayed have demonstrated that the proposed iron ore synthesis pathway is economically favored than its equivalent and shows excellent promise as a viable alternative for small-medium FT practitioners. The overall steps in the catalyst synthesis for the proposed iron ore synthesis route are also shorter than the conventional one and thus much cheaper and easier to implement.

4. Conclusions

The present study proposes a facile and cost-effective FT catalyst development, scalable and suited for fixed bed reactor operations. The proposed manufacturing costing approach enables better R&D decisions by providing a comprehensive comparative techno-economic analysis of a new catalyst formulation versus the traditional one for small-to-medium FT practitioners. The outcomes achieved in this work are promising and can be summarized in the following ways;

The textural properties were slightly inferior to other iron ores reported in the literature but still efficient for FT reactions. Its measured compressive mechanical strength of 1832.67 kPa exceeded the 620 kPa recommended crushing strength and thus deemed suited for FT fixed bed applications. A combination of Weibull statistics and

other statistical methods such as the Kruskal and Post Dunn tests approach is a sound approach to identify the best catalysts to run for a reaction where time constraints are an issue.

Table 5: A comparative summary of the conventional catalyst synthesis route versus the proposed iron ore method.

Iron ore catalysts synthesis		Convention iron catalyst synthesis	
Precursor costs (Material costs)			
Material	**US$/Kg**	**Material**	**US$/Kg**
Fresh iron	0.087	Iron (III) nona nitrate	3.13
Copper (II) nitrate trihydrate	4.81	Copper (II) nitrate trihydrate	1.10
Potassium Carbonate	2.31	Potassium Carbonate	0.53
Bentonite Binder	0.032	Silica gel	7.43
Total	**7.25**		**12.20**
Process Synthesis Costs			
Step Name	**US$/Kg**	**Step Name**	**US$/Kg**
Balling forming	4.16	Balling forming	4.16
Scrubber	3.12	Scrubber	3.12
Kiln Batch (300-1290 °C)	1.46	Kiln Batch (300-1290 °C)	1.46
Dryer Rotary(40-100°C)	6.24	Dryer Rotary(40-100°C)	6.24
Total	**18.10**	Filter Plate and frame	3.12
		Filter rotary vacuum	3.12
		Crystallizer	4.16
		Total	**34.74**
Other Expenses			
Item List	**US$/Kg**	**Item List**	**US$/Kg**
General Admin	1.27	General Admin	2.21
Research	1.33	Research	2.33
Spent Catalyst disposal	0.98	Spent Catalyst disposal	1.71
Spent catalyst recovery	1.04	Spent catalyst recovery	3.83
Selling Margin	8.52	Selling Margin	14.89
Total	**13.1**		**24.97**

The iron ore's FT catalytic performance exhibited a CO conversion of 72.1% ±4.24**,** with WGS and C_{5+} selectivity 48.6% ±1.96 and 83.2%± 5.24, respectively. This was comparable to similar work reported by other researchers in the literature, and it was found to be effective in catalyzing FT reactions. However, iron ore LTFT application is still in its infancy. Therefore, it needs more research to improve its yield and build a strong case as a viable substitute for precipitated iron catalysts.

The cost to synthesis iron ore was 46% cheaper than the traditional precipitated iron catalyst pathway and promising for small-medium FT practitioners with a limited budget. The process synthesis step in both estimations was the main contributor to the overall cost of catalyst manufacturing because it comprises the equipment needed to achieve this analysis. The step-based catalyst cost analysis approach is quick, easy, and cheap to perform without sophisticated software such as Aspen to achieve the same results. The proposed synthesis pathway was to have fewer process steps and more attractive for researchers at the early stages of catalyst design and development.

Acknowledgments

The successful completion of this work was made possible because of the financial support of the National Research Foundation of South Africa (NRF, UID 113648 and 132152) and Zhijiang College of Zhejiang University of Technology (China, Grand ID: WQ2017330434). Also, the authors appreciate Anglo American South Africa for providing iron ore gratuitous and offering their guidance and facilities for pelletizing the proposed catalyst.

References

[1] Baddour FG, Snowden-swan L, Super JD, Van Allsburg KM. Estimating Precommercial Heterogeneous Catalyst Price: A Simple Step-Based Method. Org. Process Res. Dev. 2018; 22: pp. 1599-1605. https://doi.org/10.1021/acs.oprd.8b00245

[2] Anderson J. Determining Manufacturing Costs. 2009; 1: pp. 27-31.

[3] Anderson J, Fennell A, Chemical D. Calculate Financial Indicators to Guide Investments. 2013.

[4] Desai MB. Appendix 1 Equipment cost Estimates. 1981; pp. 65-70.

[5] Mbele P. Pelletizing of Sishen concentrate. J. South. African Inst. Min. Metall. 2012; 112(3): pp. 221-228.

[6] Klerk D. Fischer Tropsch Refining. Wiley-VCH, 2011.

[7] Peters KD. Timmerhaus M. S. Plant Design and Economics for Chemical Engineers, 5th ed. New York: McGraw-Hill, 2003.

[8] Luque R, De La Osa AR, Campelo JM, Romero AA, Valverde JL, Sanchez P. Design and development of catalysts for Biomass-To-Liquid-Fischer-Tropsch (BTL-FT) processes for biofuels production. Energy Environ. Sci. 2012; 5(1): pp. 5186-5202, https://doi.org/10.1039/C1EE02238E

[9] Perego C. Development of a Fischer-Tropsch catalyst: From laboratory to commercial scale demonstration. Rend. Lincei, 2007; 18(4): pp. 305-317. https://doi.org/10.1007/BF02934926

[10] Dry ME. Handbook of Heterogenous Catalysis. 2005.

[11] Mubenesha S. A Design AND Development of iron ore Fischer Tropsch Catalyst. University of South Africa, Pretoria, 2021.

[12] Argyle MD, Bartholomew CH. Heterogeneous catalyst deactivation and regeneration: A review. Catalysts, 2015; 5(1): MDPI AG, pp. 145-269. https://doi.org/10.3390/catal5010145

[13] Badoga S, Vosoughi V, Dalai AK. Performance of Promoted Iron/CNT Catalyst for Fischer-Tropsch Synthesis: Influence of Pellet Shapes and Binder Loading. Energy and Fuels, 2017; 31(11): pp. 12633-12644. https://doi.org/10.1021/acs.energyfuels.7b01318

[14] Seo JH, *et al*. Influence of Binder on Fe-based Extrudate as Fischer-Tropsch Catalysts. Korean Chem. Eng. Res. 2011; 49(6): pp. 726-731. https://doi.org/10.9713/kcer.2011.49.6.726

[15] David E. Mechanical strength and reliability of the porous materials used as adsorbents/ catalysts and the new development trends. Arch. Mater. Sci. Eng. 2015: 73(1): pp. 5-17.

[16] Rytter E, Holmen A. Deactivation and regeneration of commercial type fischer-tropsch co-catalysts-A mini-review. Catalysts, 2015; 5(2): MDPI AG, pp. 478-499. https://doi.org/10.3390/catal5020478

[17] Zakeri M, Samimi A, Shafiee Afarani M, Salehirad A. Effects of porosity and pore size distribution on mechanical strength reliability of industrial-scale catalyst during preparation and catalytic test steps. Part. Sci. Technol. 2018; 36(1): pp. 96-103. https://doi.org/10.1080/02726351.2016.1220437

[18] Li Y, *et al*. Measurement and statistics of single pellet mechanical strength of differently shaped catalysts. Powder Technol. 2000; 113(1-2): pp. 176-184. https://doi.org/10.1016/S0032-5910(00)00231-X

[19] Bae JS, *et al*. Eco-friendly prepared iron-ore-based catalysts for Fischer-Tropsch synthesis. Appl. Catal. B Environ. 2019; 244: pp. 576-582. https://doi.org/10.1016/j.apcatb.2018.11.082

[20] U. Nations Report W. population Prospects. Department of Economic and Social Affairs Population Division. New York, 2019.

[21] Gruber H, *et al*. Fischer-Tropsch products from biomass-derived syngas and renewable hydrogen. Biomass Convers. Biorefinery, 2019. https://doi.org/10.1007/s13399-019-00459-5

[22] Hensen EJM, Wang P, Xu W. Research Trends in Fischer--Tropsch Catalysis for Coal to Liquids Technology. Front. Eng. Manag. 2016; 3(4): p. 321. https://doi.org/10.15302/J-FEM-2016051

[23] Zhang Q, Deng W, Wang Y. Recent advances in understanding the key catalyst factors for Fischer-Tropsch synthesis. J. Energy Chem. 2013; 22(1): pp. 27-38. https://doi.org/10.1016/S2095-4956(13)60003-0

[24] Aliyu AK, Modu B, Tan CW. A review of renewable energy development in Africa: A focus in South Africa, Egypt and Nigeria. Renew. Sustain. Energy Rev. 2018; 81(6): pp. 2502-2518. https://doi.org/10.1016/j.rser.2017.06.055

[25] Chun DH, *et al*. Brief Review of Precipitated Iron-Based Catalysts for Low-Temperature Fischer - Tropsch Synthesis. Top. Catal. 2020; no. 2.

[26] Dautzenberg FM. Characterization and Catalyst Development, 1989; 411(1): Dau.

[27] Abernethy R B. The New Weibull Handbook. 1996.

[28] Hong SY, *et al*. Nanocrystalline Iron-Ore-Based Catalysts for Fischer-Tropsch Synthesis. J. Nanosci. Nanotechnol. 2016; 16(2): pp. 2014-2018. https://doi.org/10.1166/jnn.2016.12002

[29] Qi W, Sathre R, III WRM, Shehabi A. Unit price scaling trends for chemical products. Lbnl-189844. 2015; 11: p. 17. https://doi.org/10.2172/1236367

[30] Weaver KF, Morales VC, Dunn SL, Godde K, Weaker PF. An Introduction to Statistical Analysis in Research: With Applications in the Biological and Life Science; John Wiley & Sons, First Edition; NW, USA; 2018; pp 353-392. https://doi.org/10.1002/9781119454205

Supplementary Data

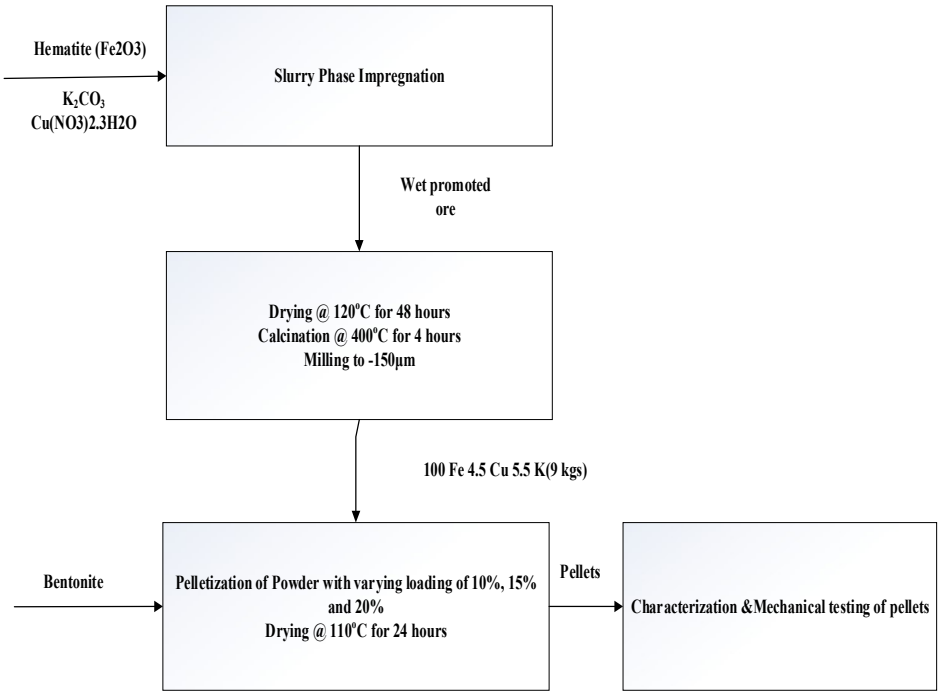

Figure S1: Depicts the overall catalyst design of the present stud.

Table S1: Single pellet crushing strengths measurements (Raw data).

Sample No.	Dry Strength (N/Pellet)		
	10% Binder Addition	15% Binder Addition	20%Binder Addition
1	25.7	22.35	22.40
2	30.95	15.80	31.20
3	47.95	17.25	18.05
4	47.95	19.00	16.60
5	17.10	23.35	18.95
6	15.30	12.65	32.30
7	21.75	18.40	21.30
8	31.00	21.20	20.70
9	23.20	26.15	22.00
10	30.65	15.80	22.95
11	45.05	13.40	15.95
12	36.05	7.10	18.65
13	53.35	20.30	19.00
14	39.40	29.95	22.75
15	33.50	22.65	21.35
16	29.25	24.05	27.45
17	42.00	17.35	19.65
18	32.60	19.05	23.65
19	27.15	19.20	21.35
20	28.10	18.30	19.25
STANDARD DEVIATION, σ	10.43	5.01	4.30
VARIANCE, σ^2	108.75	25.60	18.46
MEAN, X	32.90	19.17	21.78

Table S2: Physical properties of catalyst (Fe/K/Cu) with a binder (B) before reduction.

Catalyst	Density (Kg/m^3)	Force measurement by Force gauge(N)	Average Single Pellet Crushing Strength (kPa)	Porosity (%)
10B	4329	32.9±10.43	1833± 581.00	1.43
15B	4210	19.19± 5.01	1069± 279.08	1.85
20 B	4133	21.78±4.30	1213± 239.53	1.86

Note: 0B single pellet crushing strength (SPCS) of 0B could not be determined because the promoted ore(0B) could not make a pellet without binder addition.

Table S3: Kruskal Wallis Test & Post hoc Dunn Test Results.

Statistical Parameter	Kruskal Wallis Test results	Post hoc Dunn Test Results (Group comparison) SPCS OF 10B versus 15B	SPCS OF 10B versus 20B	SPCS OF 15B versus 20B
Chi Squared	29.1	-	-	-
Df	2	-	-	-
P-value	4.835 e^-07	0.00	0.00	0.12

Table S4: Weibull Distribution parameters calculated using estimators.

Failure probability (P) =(i-0.5)/n	Single Pellet crushing strengths for 10B(N/Pellet)	Single Pellet crushing strengths for 15B (N/Pellet)	Single Pellet crushing strengths for 20B (N/Pellet)
0.025	15.3	7.1	15.95
0.075	17.1	12.65	16.6
0.125	21.75	13.4	18.05
0.175	23.2	15.8	18.65
0.225	25.7	15.8	18.95
0.275	27.15	17.25	19
0.325	28.1	17.35	19.25
0.375	29.25	18.3	19.65
0.425	30.65	18.4	20.7
0.475	30.95	19	21.3
0.525	31	19.05	21.35
0.575	32.6	19.2	21.35
0.625	33.5	20.3	22
0.675	36.05	21.2	22.4
0.725	39.4	22.35	22.75
0.775	42	22.65	22.95
0.825	45.05	23.35	23.65
0.875	47.95	24.05	27.45
0.925	47.95	26.15	31.2
0.975	53.35	29.95	32.3

Table S5: Depicts the calculation of the size parameters of each binder loading.

10%Binder	15%Binder	20%Binder
-3.67 ln (F_0) = -13.2	-3.94 ln(Fo) = -12.03	-6.19 ln(Fo) = -19.52
Fo= e^[(-13.2)/(-3.67)]	Fo = e^[(-12.03)/(-3.94)]	Fo = e^[(-19.52)/(-6.19)]
= 40.68 N(2266.04 kPa)	= 21.19 N (1180.37 kPa)	= 23.42 N(1304.59 kPa)

Table S6: XRF results of the catalysts.

Chemical	Weight percentage (wt %)		
	Raw iron ore	0% binder Catalyst	10% binder catalysts
Fe_2O_3	95.20	89.60	85.00
K_2O	0.04	6.41	5.23
Na_2O	0.09	0.03	0.22
Al_2O_3	1.36	0.55	2.08
SiO_2	3.29	1.42	5.32
MgO	0.05	0.04	0.30
CuO	0.09	1.93	1.92

Table S7: Depicts the chemical composition of bentonite (binder).

Chemical	Weight percentage (wt %)
TiO_2	0.23
CaO	0.91
Fe_2O_3	3.96
K_2O	0.79
Na_2O	2.71
Al_2O_3	21.05
SiO_2	70.35

Average Single Pellet Crushing test conversion into Kilopascals (Kpa)

10% Binder loading Single pellet crushing strength

$\tau_s = \frac{2.8 \times 32.9}{(\pi)\ 0.004^2} = 1832.67$ kPa

15% Binder loading Single pellet crushing strength

$\tau_s = \frac{2.8 \times 19.19}{(\pi)\ 0.004^2} = 1068.96$ kPa

20% Binder loading Single pellet crushing strength

$\tau_s = \frac{2.8 \times 21.78}{(\pi)\ 0.004^2} = 1213.24$ kPa

Porosity Calculations

Porosity (%) = $(Density\ X\ single\ pore\ volume)\ x\ 100$

10% Binder loading porosity

$$\text{Porosity}(\Phi) = \frac{0.0033 \times 4329}{1000} \text{ x } 100$$

$$= 1.43\%$$

15% Binder loading porosity

$$\text{Porosity}(\Phi) = \frac{0.044 \times 4210}{1000} \text{ x } 100$$

$$= 1.85\%$$

20% Binder loading porosity

$$\text{Porosity}(\Phi) = \frac{0.045 \times 4133}{1000} \text{ x } 100$$

$$= 1.86\ \%$$

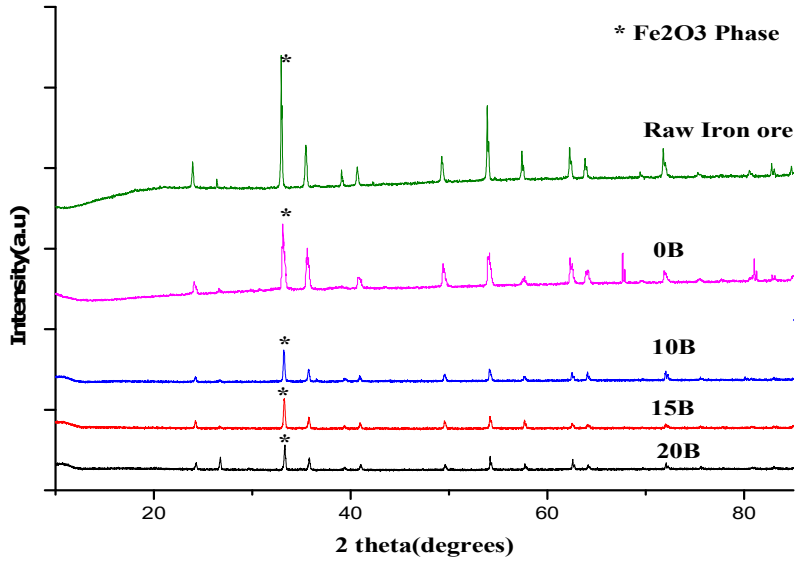

Figure S2: The diffraction patterns of the catalysts.

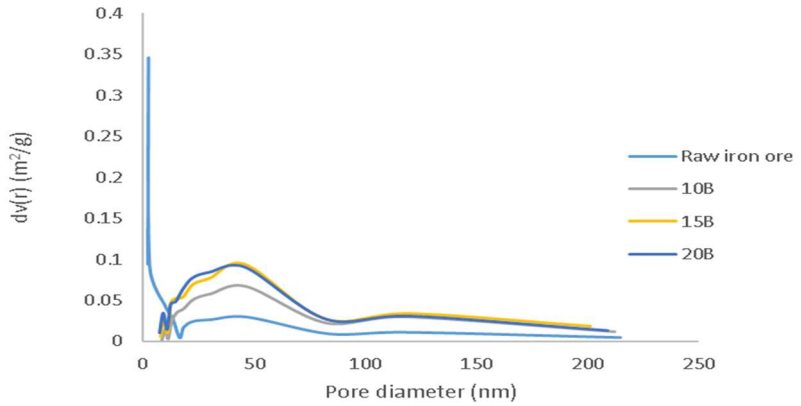

Figure S3: Pore size distributions of catalysts during synthesis.

LIST OF ABBREVIATIONS

Afrox	African Oxygen Limited
BET	Brunauer-Emmett-Teller
CO	Carbon monoxide
CAT	Catalyst
C5+	All hydrocarbons with a carbon of 5 or more
FBR	Fixed bed reactor
Fe	Iron
FID	Flame ionisation detector
FR	Flow rate
FT	Fischer Tropsch
FTS	Fischer Tropsch synthesis
GC	Gas chromatograph
GHSV	Gas hourly space velocity
GTL	Gas to liquid

H2	Hydrogen
HTFT	High temperature Fischer Tropsch
ID	Internal diameter
IO	Promoted Iron (No binder)
K	Potassium
mol/min	Mole per minute
LTFT	Low Temperature Fischer Tropsch
N2	Nitrogen
NL	Normal Litres
NTP	Normal temperature and pressure
OD	Outside diameter
Pre	Pressure
PFe	Precipitated Iron Catalyst
PIO	Promoted iron ore pellets
TCD	Thermal conductivity detector
TEM	Transmission electron microscopy
TGA	Thermo gravimetric analysis
TOS	Time on stream
TPR	Temperature-programmed reduction
UHP	Ultra-high purity
XRD	X-ray diffraction
XRF	X-ray Fluoresce
TPR	Temperature Programmed Reduction
WGS	Water Gas shift
0(B)	Binder free promoted iron ore catalyst
10(B)	10 % by weight binder addition promoted iron ore catalyst
15(B)	15 % by weight binder addition promoted iron ore catalyst
20(B)	20 % by weight binder addition promoted iron ore catalyst